

Non-Hermiticity induces localization: good and bad resonances in power-law random banded matrices

Giuseppe De Tomasi¹ and Ivan M. Khaymovich^{2,3}

¹*Department of Physics, University of Illinois at Urbana-Champaign, Urbana, Illinois 61801-3080, USA*

²*Nordita, Stockholm University and KTH Royal Institute of Technology Hannes Alfvéns väg 12, SE-106 91 Stockholm, Sweden*

³*Institute for Physics of Microstructures, Russian Academy of Sciences, 603950 Nizhny Novgorod, GSP-105, Russia*

The power-law random banded matrix (PLRBM) is a paradigmatic ensemble to study the Anderson localization transition (AT). In d -dimension the PLRBM are random matrices with algebraic decaying off-diagonal elements $H_{\mathbf{nm}} \sim 1/|\mathbf{n} - \mathbf{m}|^\alpha$, having AT at $\alpha = d$. In this work, we investigate the fate of the PLRBM to non-Hermiticity. We consider the case where the random on-site diagonal potential takes complex values, mimicking an open system, subject to random gain-loss terms. We provide an analytical understanding of the model by generalizing the Anderson-Levitov resonance counting technique to the non-Hermitian case. This generalization identifies two competing mechanisms due to non-Hermiticity: one favoring localization and the other delocalization. The competition between the two gives rise to AT at $d/2 \leq \alpha \leq d$. The value of the critical α depends on the strength of the on-site potential, reminiscent of Hermitian disordered short-range models in $d > 2$. Within the localized phase, the wave functions are algebraically localized with an exponent α even for $\alpha < d$. This result provides an example of non-Hermiticity-induced localization.

Introduction – Random matrix theory (RMT) is a resounding resource to tackle problems in several contexts, ranging from nuclear physics to number theory [1–4]. In disordered quantum systems, RMT has been widely used in the context of Anderson localization (AL) and quantum chaos [3–7]. For instance, the Anderson transition (AT) has been successfully studied using the so-called power-law random banded matrix (PLRBM) ensemble [8]. In d -dimensions, the PLRBM are random matrices in which off-diagonal elements decay algebraically with the distance, $H_{\mathbf{nm}} \sim \frac{1}{|\mathbf{n}-\mathbf{m}|^\alpha}$. The spatial structure of the PLRBM allows a complete solution in terms of resonance counting, resolved over spatial distance [9], renormalization group (RG) [10], and non-linear sigma model [8], finding AT, at $\alpha_{AT} = d$, separating an ergodic phase from a localized one. That makes the PLRBM a fantastic toolbox for understanding universal properties in disordered quantum systems.

From a different perspective, non-Hermitian quantum systems have recently attracted significant attention. Non-Hermitian terms originated as an effective theory to describe system couples to baths and reservoirs. Non-Hermiticity leads to a unique and broad phenomenology, ranging from skin effect, measurement-induced transition, and generalized topology [11–28]. In disordered systems, non-Hermiticity has drastic effects. In general, non-Hermiticity enhances decoherence and might break localization. The most well-known example is a so-called Hatano-Nelson model [29] which shows that even in one dimension, where the short-range Hermitian system is localized for any amount of disorder, strong non-Hermiticity breaks AL. Consequently, non-Hermiticity might fundamentally change the AT universality classes [30–32].

In this work, we take the root of studying AL in non-Hermitian systems using RMT techniques. In particu-

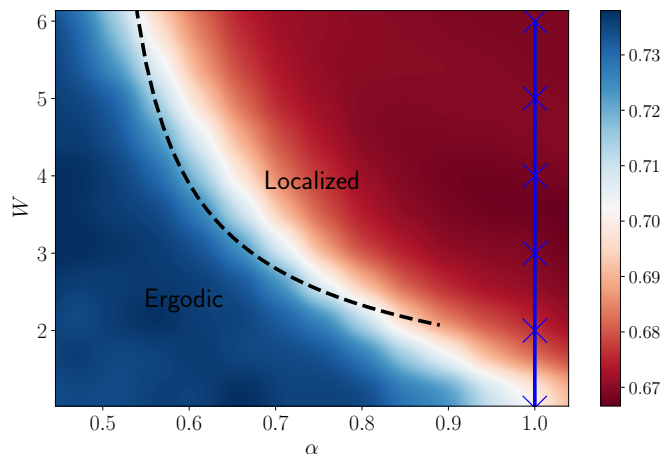


FIG. 1. **Phase diagram of the non-Hermitian PLRBM with random gain-loss terms in $d = 1$ dimension**, showing the averaged spectrum gap ratio r vs the algebraic-decay rate α of the hopping terms and the diagonal disorder amplitude W . $\bar{r} = 2/3$ for localized systems and $\bar{r} \approx 0.738$ for ergodic ones. For the Hermitian case, the transition happens at $\alpha = 1$ for any W (vertical blue line). The dashed line is the analytical prediction for AT.

lar, we investigate a non-Hermitian deformation of the PLRBM model. We break the Hermiticity by adding a complex on-site disorder but leaving Hermitian off-diagonal elements. Several works have considered this type of non-Hermiticity [25–27, 31, 33–37], and this choice mimic a system subject to local random gain-loss.

We show that Hermiticity-breaking terms change the phase diagram of the PLRBM, see Fig. 1. Unexpectedly, unlike the previous results, we found that non-Hermiticity enhances localization. Using analytical and numerical techniques, we provide evidence that AT shifts to smaller values $d/2 < \alpha_c(W) \leq d$ and depends on

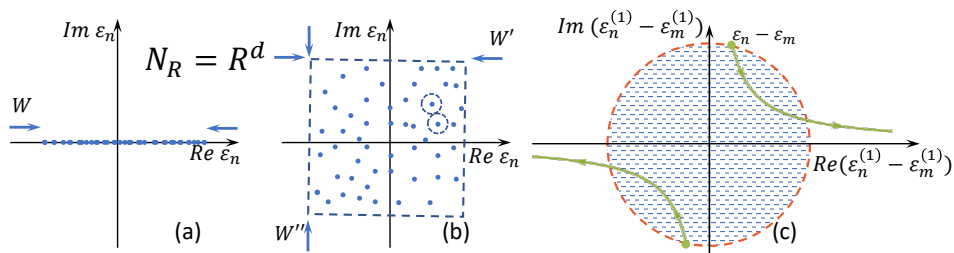


FIG. 2. **Structure of resonances.** (a) The level spacing in the Hermitian case, Eq. (5), is determined by the ratio of the energy interval W and the number of lattice sites $N_R \sim R^d$ at the distance R from a certain point. (b) In the non-Hermitian case, the complex (2d) distribution of ε_n leads to the mean area per level $A_R \simeq W^2/R^d$, Eq. (8) and (c) the hybridization of levels, Eq. (10), may lead to the attraction between levels (shaded region), while the hopping term increases (green arrows).

the strength of the on-site disorder W . To understand this counter-intuitive phenomenon, we generalize the Anderson-Levitov resonance counting and hybridization of resonant-level pairs, like in the standard RG [9, 10]. We uncover the competition of two mechanisms due to non-Hermiticity, favoring localization and delocalization, respectively. The complex-valued diagonal potential, unlike the real-valued one, Fig. 2(a), forms an effectively two-dimensional distribution [36], Fig. 2(b), which increases the level spacing parametrically in system size and suppresses the number of resonances. However, non-Hermiticity also induces a unique attraction between resonant levels, hybridizing them, Fig. 2(c), which forms the so-called “bad” resonances. The level attraction, caused by the non-Hermitian terms, breaks the central assumption of spatial RG and dramatically changes the phase diagram. As a result, non-Hermiticity drives a new kind of transition that depends on the strength of on-site potential, like in short-range models in $d > 2$. In addition, for the non-Hermitian PLRBM, we show that the localized phase has an algebraic nature also for $\alpha \leq d$, which is forbidden in its Hermitian counterpart.

Model & Methods – PLRBM in d -dimensions reads as

$$H_{\mathbf{m}\mathbf{n}} = \varepsilon_{\mathbf{n}}\delta_{\mathbf{m}\mathbf{n}} + j_{\mathbf{m}\mathbf{n}}, \quad (1)$$

where $\varepsilon_{\mathbf{n}}$ and $j_{\mathbf{m}\mathbf{n}} = j_{\mathbf{n}\mathbf{m}}^*$ are independent complex-valued box-distributed random variables with zero mean and the amplitudes

$$|\operatorname{Re} \varepsilon_{\mathbf{n}}|, |\operatorname{Im} \varepsilon_{\mathbf{n}}| \leq W, \quad (2a)$$

$$|\operatorname{Re} j_{\mathbf{m}\mathbf{n}}|^2, |\operatorname{Im} j_{\mathbf{m}\mathbf{n}}|^2 \leq \frac{1}{2(|\mathbf{m} - \mathbf{n}|^2 + b^2)^\alpha}, \quad (2b)$$

\mathbf{m} is a radial vector of a lattice in \mathbb{Z}^d . W is the on-site disorder strength, α – the power of the off-diagonal power-law decay, and b is the bandwidth of the decay. For simplicity, we restrict our consideration to $d \leq 2$, where short-range models ($\alpha \rightarrow \infty$) are localized for any amount of disorder, and take $b \lesssim 1$. The non-Hermiticity is provided by the complex-valued diagonal term $\varepsilon_{\mathbf{m}} \in \mathbb{C}$.

We now briefly summarize the localization phase diagram of the Hermitian PLRBM. The model hosts AT

at $\alpha = d$, independent of the parameters W and b . For $\alpha < d$, the wave function are extended and ergodic, and, for $\alpha < d/2$, the wave function statistics coincides with the Porter-Thomas distribution of RMT. At the transition, the eigenstates show multifractality, weak for $b \gg 1$ and strong for $b \ll 1$ [6]. In the localized phase ($\alpha > d$), the wave functions are power-law localized, and the wave function decay rate coincides with α . The transition is understood using the so-called Anderson-Levitov resonance counting [9] with an RG approach [10]. The starting point is the perturbative *locator expansion*

$$\psi_{\mathbf{n}}(\mathbf{m}) = \delta_{\mathbf{m}\mathbf{n}} + \frac{j_{\mathbf{m}\mathbf{n}}}{\varepsilon_{\mathbf{n}} - \varepsilon_{\mathbf{m}}} + \dots \quad (3)$$

which converges, if most of the site pairs \mathbf{m} and \mathbf{n} are not in resonance, $\left| \frac{j_{\mathbf{m}\mathbf{n}}}{\varepsilon_{\mathbf{n}} - \varepsilon_{\mathbf{m}}} \right| < 1$. To find AT, one should count the number $N_{res, \mathbf{n}}$ of resonant pairs $\left| \frac{j_{\mathbf{m}\mathbf{n}}}{\varepsilon_{\mathbf{n}} - \varepsilon_{\mathbf{m}}} \right| > 1$ for each $\psi_{\mathbf{n}}$ state. For $N_{res, \mathbf{n}} \lesssim O(N^0)$ the perturbation theory is stable and the state is localized, otherwise for $N_{res, \mathbf{n}} \gtrsim O(N^{c>0})$ the state delocalizes. At each i th step of the spatial RG [9, 10], when $|\mathbf{m} - \mathbf{n}| \equiv R$ is in a ring

$$R_i < R < 2R_i \equiv R_{i+1}, \quad (4)$$

one can count the number of resonances by comparing the mean-level spacing in the d -dimensional ring [38]

$$\delta_R = \frac{W}{R^d}, \quad (5)$$

with the hopping term $j_{\mathbf{m}\mathbf{n}} \sim 1/R^\alpha$ and progressively increase the distance at each step. Thus, for all $\alpha > d$ and large enough distances $R \gtrsim (1/W)^{1/(\alpha-d)} \sim O(1)$ there are no resonances as $\delta_R/j_R = WR^{\alpha-d} > O(1)$. $(1/W)^{1/(\alpha-d)}$ is the radius beyond which the resonances are absent. We can estimate the number of sites resonant to the state $\psi_{\mathbf{n}}(\mathbf{m})$ as $\sim (1/W)^{d/(\alpha-d)}$. For these resonant sites, one cannot use the perturbation theory but instead must use its degenerate counterpart. However, the hybridization of these resonance pairs does not produce other resonance pairs. As a result, for $\alpha > d$ the number or resonant pair is bounded with system size. Instead,

$\alpha < d$ the resonances proliferate at large enough distances $R > R_c \simeq W^{1/(d-\alpha)}$, as $j_R/\delta_R \sim R^{(d-\alpha)}/W > 1$. The number of such resonances at a distance R grows as

$$N_{res,\mathbf{n}}(R) \simeq \frac{j_R}{\delta_R} \sim \frac{R^{d-\alpha}}{W}, \quad (6)$$

leading to

$$N_{res,\mathbf{n}} = \sum_i N_{res,\mathbf{n}}(R_i) \sim N^{d-\alpha} \gg N^0. \quad (7)$$

This argument shows that for $\alpha < d$ the number of resonances diverges with system size N . Therefore AT in the Hermitian PLRBM happens at $\alpha_{AT} = d$ and does not depend on W nor b .

Non-Hermitian case – Next, we generalize the Anderson-Levitov resonance counting to the non-Hermitian case. Following the same steps like in the Hermitian case, we subdivide the space in concentric rings around a lattice point \mathbf{n} , Eq. (4), and compare the hopping term $j_R \sim 1/R^\alpha$ with the mean level spacing δ_R .

As the complex potential, Eq. (2a), has a 2d nature [37], the mean level spacing is given by the root of the ratio between the entire available area $\sim W^2$ and the number of sites in the ring $\sim R^d$, see Fig. 2(b),

$$\delta_R^{nH} \sim \frac{W}{R^{d/2}}, \quad (8)$$

thus it decays parametrically slower than in the Hermitian case in Eq. (5). Focusing only on the increase of the level spacing, one might be tempted to conclude that the system is clearly more localized, compared to the Hermitian one and the AT should be at $\alpha_{AT} = d/2$.

However, as we observe numerically in Figs. 1 and 5, the transition happens at $d/2 \leq \alpha_{AT}(W) \leq d$, which is W -dependent. We show that this is due to the level hybridization, which, in contrast to the Hermitian case, may enhance delocalization by level attraction. Let's consider the structure of a single resonance for both real and complex $\varepsilon_{\mathbf{n}}$ and Hermitian hopping $j_{\mathbf{nm}} = j_{\mathbf{mn}}^*$.

In the resonance condition $|\varepsilon_{\mathbf{m}} - \varepsilon_{\mathbf{n}}| < |j_{\mathbf{nm}}|$ for two sites \mathbf{n} and \mathbf{m} , following the degenerate perturbation theory, one should diagonalize a 2×2 matrix

$$\begin{pmatrix} \varepsilon_{\mathbf{m}} & j_{\mathbf{mn}} \\ j_{\mathbf{nm}} & \varepsilon_{\mathbf{n}} \end{pmatrix}, \quad (9)$$

leading to the "renormalized" on-site energies

$$\varepsilon_{\mathbf{m},\mathbf{n}}^{(1)} = \frac{\varepsilon_{\mathbf{m}} + \varepsilon_{\mathbf{n}}}{2} \pm \sqrt{\left(\frac{\varepsilon_{\mathbf{m}} - \varepsilon_{\mathbf{n}}}{2}\right)^2 + |j_{\mathbf{mn}}|^2}. \quad (10)$$

For the Hermitian case, with $(\varepsilon_{\mathbf{m}} - \varepsilon_{\mathbf{n}})^2 \geq 0$, we have level repulsion,

$$\left| \frac{\varepsilon_{\mathbf{m}}^{(1)} - \varepsilon_{\mathbf{n}}^{(1)}}{\varepsilon_{\mathbf{m}} - \varepsilon_{\mathbf{n}}} \right| = \sqrt{1 + \frac{|j_{\mathbf{mn}}|^2}{(\varepsilon_{\mathbf{m}} - \varepsilon_{\mathbf{n}})^2}} > 1, \quad (11)$$

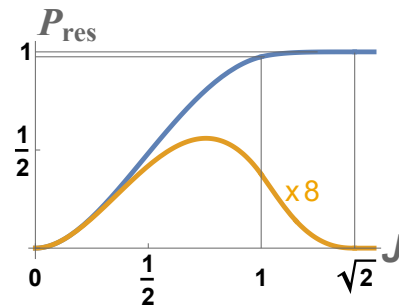


FIG. 3. Probabilities of (blue) usual P_{res} and (orange) “bad” P_{bad} resonances as functions of $J = |j_{\mathbf{mn}}|/(2W)$. The latter is multiplied by 8.

leading to the convergent RG at $\alpha > \alpha_{AT} = d$.

However, in the non-Hermitian case, the inequality in Eq. (11) is not always satisfied. The simplest example of this kind is when $(\varepsilon_{\mathbf{m}} - \varepsilon_{\mathbf{n}})^2 < 0$,

$$\left| \frac{\varepsilon_{\mathbf{m}}^{(1)} - \varepsilon_{\mathbf{n}}^{(1)}}{\varepsilon_{\mathbf{m}} - \varepsilon_{\mathbf{n}}} \right| = \left| \sqrt{1 - \left| \frac{j_{\mathbf{mn}}}{\varepsilon_{\mathbf{m}} - \varepsilon_{\mathbf{n}}} \right|^2} \right| < 1, \quad (12)$$

for all $j_{\mathbf{mn}}^2 < 2|\varepsilon_{\mathbf{m}} - \varepsilon_{\mathbf{n}}|^2$. We refer to this level attraction as “bad” resonances. It is this new phenomenon of level attraction, Fig. 2(c), which competes with the enhanced mean level spacing δ_R^{nH} and breaks the RG steps at $d/2 < \alpha < \alpha_{AT}(W)$ as soon as the probability of such “bad” resonances is significantly large. Crucially, these “bad” resonances appear with a finite (but small) probability per eigenstate, which we next calculate.

We parameterize the hopping $|j_{\mathbf{mn}}| = 2WJ$ and diagonal elements with real parameters J, X, Y, x, y

$$\frac{\varepsilon_{\mathbf{m}}}{W} = X + iY + x + iy, \quad \frac{\varepsilon_{\mathbf{n}}}{W} = X + iY - x + iy, \quad (13)$$

and rewrite the “bad”-resonance condition, Eq. (11), as

$$(x^2 + y^2) < J^2 < 2(y^2 - x^2). \quad (14)$$

For a fixed J one can straightforwardly calculate the probability of the usual resonances P_{res} , defined as the conditional integral $J^2 > (x^2 + y^2)$ over the parameters X, Y, x , and y , which is present also in the Hermitian case. The one of “bad” resonances P_{bad} , being the attribute of non-Hermitian case, we calculate via the integral over (14). The exact definitions and expressions of both probabilities are given in the Supplemental Material [39], while here we show only their plots vs J , Fig. 3. One immediately sees that at large hopping $J > \sqrt{2}$, when P_{res} goes to 1, P_{bad} disappears.

The number of resonances in both cases is given by the summation over the distances R and the integration over the random-amplitude $|s_{\mathbf{m},\mathbf{m}+\mathbf{R}}| \equiv s$ distribution (being box for $\text{Re } s_{\mathbf{mn}}$ and $\text{Im } s_{\mathbf{mn}}$ in Eq. (2b), with $s \leq 1$):

$$J_{\mathbf{m},\mathbf{m}+\mathbf{R}} = \frac{|s_{\mathbf{m},\mathbf{m}+\mathbf{R}}|}{2WR^\alpha}. \quad (15)$$

For $W > 1/2$, and $d = 1$, one obtains the number of the usual and “bad” resonances per eigenstate to be [39]

$$N_{res} = \sum_{\mathbf{R}} \int P_{res} \left(J_{\mathbf{m}, \mathbf{m}+\mathbf{R}} = \frac{s}{2WR\alpha} \right) P(s) ds \approx \\ \approx 1.05 \frac{\zeta_{2\alpha}}{W^2} - 0.61 \frac{\zeta_{3\alpha}}{W^3} + 0.08 \frac{\zeta_{4\alpha}}{W^4} \quad (16)$$

$$N_{bad} = \sum_{\mathbf{R}} \int P_{bad} \left(J_{\mathbf{m}, \mathbf{m}+\mathbf{R}} = \frac{s}{2WR\alpha} \right) P(s) ds \approx \\ \approx 0.13 \frac{\zeta_{2\alpha}}{W^2} - 0.09 \frac{\zeta_{3\alpha}}{W^3} + 0.01 \frac{\zeta_{4\alpha}}{W^4}, \quad (17)$$

where ζ_x is the zeta function, which converges at $x > 1$. As a result, both N_{res} and N_{bad} are finite at $\alpha > d/2$. If one neglects the contribution of “bad” resonances, Eq. (16) implies that the localization happens at $\alpha > d/2$. However, the number of “bad” resonances breaks down the entire RG analysis by enabling an avalanche of higher-order resonances. Therefore, localization in the non-Hermitian case is achieved only at $N_{bad} \ll 1$ per eigenstate or at $N_{bad} \cdot N$ resonances in the entire system. From the numerical results, we find the transition at

$$N_{bad}(W, \alpha) \simeq N_c \equiv 0.045, \quad (18)$$

which immediately makes the critical exponent $a_c(W)$ to be strongly dependent on W via Eq. (17).

Numerical results – In the numerical simulations we focus on $d = 1$, minimizing finite-size effects and on Hermitian complex-valued hopping terms with the box distribution, Eq. (2b). The standard probe to characterize ergodicity and its breakdown is the spectral statistics of the model, Eq. (1). In the ergodic phase, we expect the level statistics to be close to that of the Ginibre ensemble, a non-Hermitian RMT. In the localized phase, the energy spectrum should be 2d Poisson. To separate these two limits, we study the complex gap ratio [40]

$$r_n^C = \frac{Z_n^{NN} - Z_n}{Z_n^{NNN} - Z_n}, \quad (19)$$

where $\{Z_n\}$ is the spectrum of H , which is, in general, complex, $Z_n \in \mathbb{C}$. Z_n^{NN} and Z_n^{NNN} are the nearest neighbor (NN) and the next-nearest neighbor (NNN) of Z_n with respect to the Euclidean distance in \mathbb{C} , respectively. Decomposing $r_n^C = r_n e^{i\theta_n}$, we analyze $\{r_n\}$ and $\{\theta_n\}$, separately. For Ginibre RMT $-\cos\theta \approx 0.229$ and $\bar{r} \approx 0.738$ [40], while in the localized phase, we have $-\cos\theta_n = 0$ and $\bar{r} = 2/3$. The overline indicates the average over disorder and energy spectrum.

Figures 4(a) and (b) show \bar{r} and $-\cos\theta$ as a function of α at a fixed $W = 2$, respectively. For small α , both quantities approach their RMT prediction (red dashed lines) with increasing N , while at large α , they tend to the Poisson values. An abrupt crossover between these

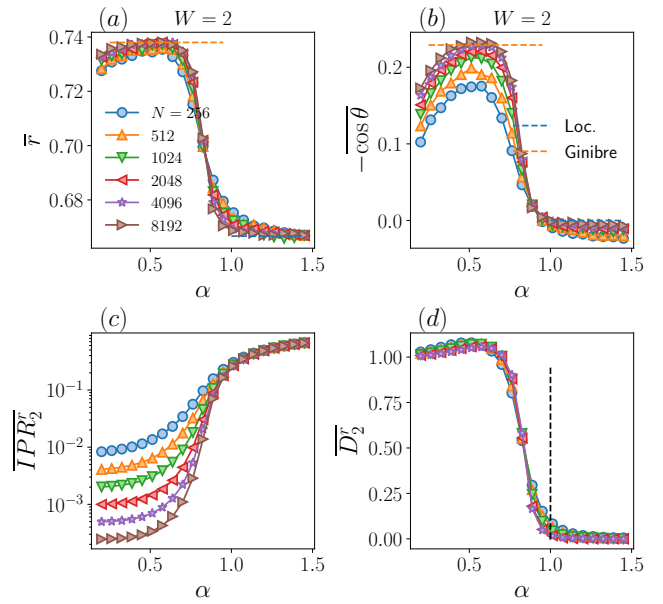


FIG. 4. (a),(b) Spectral statistics \bar{r} and $-\cos\theta$ vs α for $W = 2$ and several N . (c),(d) \overline{IPR}_2 and the respective fractal dimension \overline{D}_2^r for $W = 2$. The vertical dashed line $\alpha_{AT} = 1$ points the phase transition in the Hermitian case.

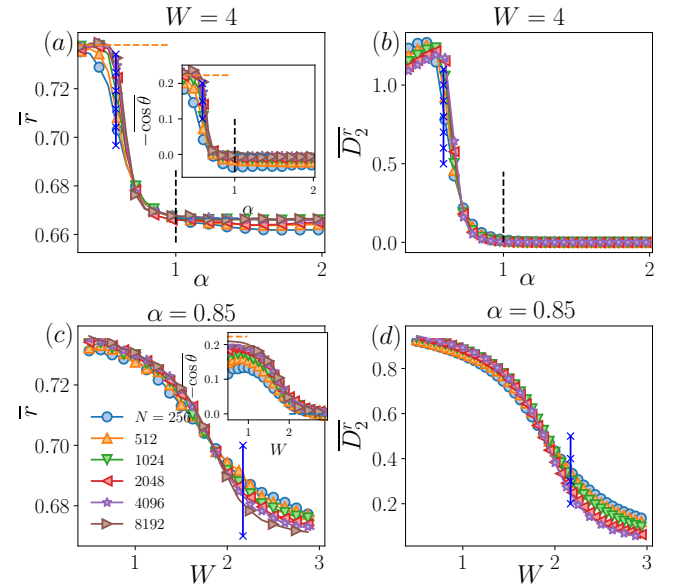


FIG. 5. (a),(b) Spectral statistics and fractal dimension vs α for $W = 4$. The vertical dashed lines at $\alpha_{AT} = 1$ point AT in the Hermitian case. (c),(d) \bar{r} , $-\cos\theta$ and \overline{IPR}_2 and \overline{D}_2^r for fixed $\alpha = 0.85$ vs the on-site disorder W . Blue vertical lines are the theoretical predictions, Eq. (17), for the critical point with (a, b) $N_{bad}(W = 4, \alpha_c) = N_c$ (c, d) $N_{bad}(W_c, \alpha = 0.85) = N_c$.

limits appears around $\alpha_c \approx 0.8 \leq \alpha_{AT} = 1$. In agreement with the analytical argument, this result points out the existence of AT, occurring at a smaller value than in the

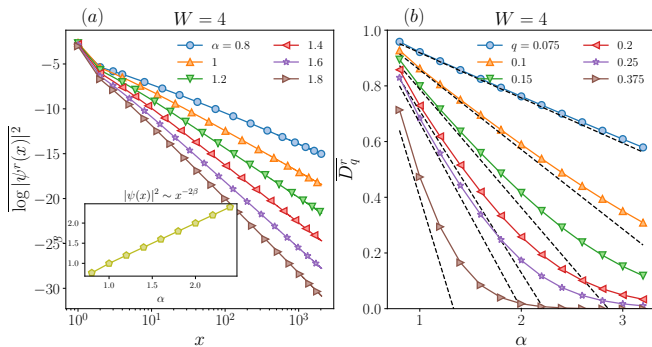


FIG. 6. (a) Eigenstate algebraic spatial decay, $\psi(x) \sim 1/x^\beta$, in log-log scale for several α and $N = 2048$. The inset in (a) shows that $\beta \approx \alpha$. (b) D_q^r vs α for several small q . The dashed lines show the analytical prediction $D_q^r = (2\alpha q - 1)/(q - 1)$.

Hermitian case.

To further support the above observation, we compute the inverse participation ratio IPR_q and extract a fractal exponent D_q^r via its scaling with the system size N

$$IPR_q^r = \sum_{\mathbf{m}} |\psi_n^r(\mathbf{m})|^{2q}, \quad D_q^r = \frac{1}{1-q} \frac{d \log IPR_q^r}{d \log N}. \quad (20)$$

Here ψ_n^r is the right eigenvector with eigenvalue Z_n [41]. $0 \leq D_q^r \leq 1$ measures the spread of the wave functions. In the ergodic phase, $D_q^r \rightarrow 1$, while in the power-law localized phase, the behavior of D_q^r depends on the power β of the decay of the wave function $\psi(\mathbf{m}) \sim 1/|\mathbf{m}|^\beta$: $D_q^r = 0$ for $q > 1/(2\beta)$, while for $q < 1/(2\beta)$ the fractal exponent is $D_q^r = (2\alpha q - 1)/(q - 1)$. Varying q in D_q^r , we can probe if the phase is power-law localized. As shown in Fig. 4 (c), $D_2^r \approx 1$ for small $\alpha < 0.85$ indicates ergodicity. For larger α , we observe that $D_2^r \rightarrow 0$. Importantly, $D_2^r \rightarrow 0$ also at $\alpha_c < \alpha < d = 1$.

Now, we focus on W -dependence of α_c . To understand the dependence of the critical point with the onsite-disorder strength, we tune W . Figure 5(a)-(b) shows \bar{r} , $-\cos \theta$ and \bar{D}_2^r at larger $W = 4$. As one can observe, the crossover between ergodic to localized takes place to a smaller power $\alpha_c(W = 4) \approx 0.72 \leq \alpha_c(W = 2)$. This suggests that the critical point, α_c , depends on W , see also Fig. 1, unlike the Hermitian counterpart. To support this conjecture, in Fig. 5(c)-(d), we show the r -statistic and fractal dimension for a fixed $\alpha = 0.85 < \alpha_{AT}$ as a function of W . As expected, with increasing system size N , the curves in Fig. 5(c)-(d) tend to their ergodic values for $W \leq 1.85$. Instead, at larger W , we observe localization. The dependence of the critical point $d/2 \leq \alpha_c \leq d$ with the disorder strength W is relatively good in agreement with the theoretical prediction in Eqs. (17), (18), see Fig. 1 and Fig. 5. In particular, we have that $\alpha_c \rightarrow 1/2$ as $1/W^2$ at large W , Fig. 1.

Having provided the evidence that the critical point depends on the strength of the on-site disorder, we turn

to the type of localization. Within the localized phase, we analyze the decay of the eigenstates from its absolute value maximum [42–48]. The wave function decay is algebraic, i.e. $|\psi(x)|^2 \sim 1/|x|^{2\beta}$, Fig. 6(a), and the power β is given by $\beta \approx \alpha$ in agreement with the non-Hermitian perturbation theory $\alpha < \alpha_c < 1$, see inset of Fig. 6(a). The algebraic nature of the localized phase manifests itself also in D_q^r vs α for several q , see Fig. 6(b). In good agreement with the theoretical prediction for power-law localized phases, $D_q^r \approx (2\alpha q - 1)/(q - 1)$ for $q < 1/(2\alpha) \approx 1/(2\beta)$ and zero otherwise.

Conclusion – In this work, we inspect the fate of the Anderson transition in a non-Hermitian PLRBM model with random gain and loss in d -dimensions. We provide numerical and analytical evidence of the existence of AT, which happens at a smaller power α than in the Hermitian counterpart.

To elaborate an analytical understanding of the system, we generalize the Anderson-Levitov resonance counting to the non-Hermitian case. This technique reveals the emergence of two competing mechanisms: the parametric enhancement of the level spacing, which enhances localization, and the emerging “bad” resonances that favor delocalization. The competition between the two leads to the Anderson transition at $d/2 \leq \alpha_c(W) \leq d$. The critical point depends on the on-site-disorder amplitude W , similar to short-range models in $d > 2$. This result should be compared to the Hermitian case, where the transition happens at $\alpha = d$ for any W . We also show that in the localized phase the wave-function envelopes decay as a power law from its maximum. The spatial decay coincides with the ones of the PLRBM hopping terms, also for $\alpha_c(W) \leq \alpha \leq d$. As a result, non-Hermitian systems might also host localized algebraic phases with a decay rate lower than d , which is forbidden in Hermitian systems.

Understanding the nature of the critical point at the transition, its dynamics, or the possible existence of non-ergodic extended states in the non-Hermitian PLRBM, and its application in many-body systems remains an objective for future study.

Acknowledgments – We thank T. Hughes and V. E. Kravtsov for illuminating discussions. I. M. K. acknowledges the support by the European Research Council under the European Union’s Seventh Framework Program Synergy ERC-2018-SyG HERO-810451. G. D. T. acknowledges the support from the EPiQS Program of the Gordon and Betty Moore Foundation.

-
- [1] Terence Tao, *Topics in random matrix theory*, Graduate Studies in Mathematics, Vol. 132 (American Mathematical Society, 2011).
 - [2] M.L. Mehta, *Random Matrices*, ISSN (Elsevier Science, 2004).

- [3] C. W. J. Beenakker, “Random-matrix theory of quantum transport,” *Rev. Mod. Phys.* **69**, 731–808 (1997).
- [4] F. Haake, *Quantum Signatures of Chaos*, Physics and astronomy online library (Springer, 2001).
- [5] P. W. Anderson, “Absence of diffusion in certain random lattices,” *Phys. Rev.* **109**, 1492–1505 (1958).
- [6] F. Evers and A. D. Mirlin, “Anderson transitions,” *Rev. Mod. Phys.* **80**, 1355 (2008).
- [7] Alexander D. Mirlin, “Statistics of energy levels and eigenfunctions in disordered systems,” *Physics Reports* **326**, 259–382 (2000).
- [8] A. D. Mirlin, Y. V. Fyodorov, F.-M. Dittes, J. Quezada, and T. H. Seligman, “Transition from localized to extended eigenstates in the ensemble of power-law random banded matrices,” *Phys. Rev. E* **54**, 3221 (1996).
- [9] L. S. Levitov, “Absence of localization of vibrational modes due to dipole-dipole interaction,” *Europhys. Lett.* **9**, 83 (1989).
- [10] L. S. Levitov, “Delocalization of vibrational modes caused by electric dipole interaction,” *Phys. Rev. Lett.* **64**, 547 (1990).
- [11] Dan S. Borgnia, Alex Jura Kruchkov, and Robert-Jan Slager, “Non-Hermitian boundary modes and topology,” *Phys. Rev. Lett.* **124**, 056802 (2020).
- [12] Nobuyuki Okuma, Kohei Kawabata, Ken Shiozaki, and Masatoshi Sato, “Topological origin of non-Hermitian skin effects,” *Phys. Rev. Lett.* **124**, 086801 (2020).
- [13] Shunyu Yao and Zhong Wang, “Edge states and topological invariants of non-Hermitian systems,” *Phys. Rev. Lett.* **121**, 086803 (2018).
- [14] M. S. Rudner and L. S. Levitov, “Topological transition in a non-Hermitian quantum walk,” *Phys. Rev. Lett.* **102**, 065703 (2009).
- [15] Yi Chen Hu and Taylor L. Hughes, “Absence of topological insulator phases in non-Hermitian PT -symmetric hamiltonians,” *Phys. Rev. B* **84**, 153101 (2011).
- [16] Kenta Esaki, Masatoshi Sato, Kazuki Hasebe, and Mahito Kohmoto, “Edge states and topological phases in non-Hermitian systems,” *Phys. Rev. B* **84**, 205128 (2011).
- [17] Zongping Gong, Yuto Ashida, Kohei Kawabata, Kazuaki Takasan, Sho Higashikawa, and Masahito Ueda, “Topological phases of non-Hermitian systems,” *Phys. Rev. X* **8**, 031079 (2018).
- [18] Henning Schomerus, “Topologically protected midgap states in complex photonic lattices,” *Opt. Lett.* **38**, 1912–1914 (2013).
- [19] Yuto Ashida, Zongping Gong, and Masahito Ueda, “Non-Hermitian physics,” *Advances in Physics* **69**, 249–435 (2020).
- [20] Nimrod Moiseyev, *Non-Hermitian Quantum Mechanics* (Cambridge University Press, 2011).
- [21] Brian Skinner, Jonathan Ruhman, and Adam Nahum, “Measurement-induced phase transitions in the dynamics of entanglement,” *Phys. Rev. X* **9**, 031009 (2019).
- [22] A. Zabalo, M. J. Gullans, J. H. Wilson, R. Vasseur, A. W. W. Ludwig, S. Gopalakrishnan, David A. Huse, and J. H. Pixley, “Operator scaling dimensions and multifractality at measurement-induced transitions,” *Phys. Rev. Lett.* **128**, 050602 (2022).
- [23] Joshua Feinberg and A. Zee, “Non-Hermitian localization and delocalization,” *Phys. Rev. E* **59**, 6433–6443 (1999).
- [24] Luca G. Molinari, “Non-Hermitian spectra and Anderson localization,” *Journal of Physics A: Mathematical and Theoretical* **42**, 265204 (2009).
- [25] Yi Huang and B. I. Shklovskii, “Anderson transition in three-dimensional systems with non-Hermitian disorder,” *Phys. Rev. B* **101**, 014204 (2020).
- [26] Yi Huang and B. I. Shklovskii, “Spectral rigidity of non-Hermitian symmetric random matrices near the Anderson transition,” *Phys. Rev. B* **102**, 064212 (2020).
- [27] Kohei Kawabata and Shinsei Ryu, “Nonunitary scaling theory of non-Hermitian localization,” *Phys. Rev. Lett.* **126**, 166801 (2021).
- [28] Emil J. Bergholtz, Jan Carl Budich, and Flore K. Kunst, “Exceptional topology of non-Hermitian systems,” *Rev. Mod. Phys.* **93**, 015005 (2021).
- [29] Naomichi Hatano and David R. Nelson, “Localization transitions in non-Hermitian quantum mechanics,” *Phys. Rev. Lett.* **77**, 570–573 (1996).
- [30] Denis Bernard and André LeClair, “A classification of non-Hermitian random matrices,” in *Statistical Field Theories*, edited by Andrea Cappelli and Giuseppe Mussardo (Springer Netherlands, Dordrecht, 2002) pp. 207–214.
- [31] Xunlong Luo, Tomi Ohtsuki, and Ryuichi Shindou, “Universality classes of the Anderson transitions driven by non-Hermitian disorder,” *Phys. Rev. Lett.* **126**, 090402 (2021).
- [32] Xunlong Luo, Zhenyu Xiao, Kohei Kawabata, Tomi Ohtsuki, and Ryuichi Shindou, “Unifying the Anderson transitions in Hermitian and non-Hermitian systems,” *Phys. Rev. Res.* **4**, L022035 (2022).
- [33] Ryusuke Hamazaki, Kohei Kawabata, and Masahito Ueda, “Non-Hermitian many-body localization,” *Phys. Rev. Lett.* **123**, 090603 (2019).
- [34] A. F. Tzortzakakis, K. G. Makris, and E. N. Economou, “Non-Hermitian disorder in two-dimensional optical lattices,” *Phys. Rev. B* **101**, 014202 (2020).
- [35] A. F. Tzortzakakis, K. G. Makris, A. Szameit, and E. N. Economou, “Transport and spectral features in non-Hermitian open systems,” *Phys. Rev. Res.* **3**, 013208 (2021).
- [36] Giuseppe De Tomasi and Ivan M. Khaymovich, “Non-Hermitian Rosenzweig-Porter random-matrix ensemble: Obstruction to the fractal phase,” *Phys. Rev. B* **106**, 094204 (2022).
- [37] G. De Tomasi and I. M. Khaymovich, “Many-body localization in gain-loss non-Hermitian systems,” (2022), in preparation.
- [38] δ_R is given by the ratio of the width of the on-site random potential $-W/2 < \varepsilon_{\mathbf{m}} < W/2$ to the number $\sim R^d$ of lattice sites in the ring (4).
- [39] See Supplemental Material at [URL will be inserted by publisher] for details of calculations of the probabilities of resonances, which includes Refs. [10].
- [40] Lucas Sá, Pedro Ribeiro, and Tomaž Prosen, “Complex spacing ratios: A signature of dissipative quantum chaos,” *Phys. Rev. X* **10**, 021019 (2020).
- [41] We have checked in the Supplemental Materials [39] that IPR is statistically the same for left eigenvectors and mixed definitions $IPR_q^r = \sum_{\mathbf{m}} |\psi_n^r(\mathbf{m}) \psi_n^l(\mathbf{m})|^q$.
- [42] X Deng, VE Kravtsov, GV Shlyapnikov, and L Santos, “Duality in power-law localization in disordered one-dimensional systems,” *Phys. Rev. Lett.* **120**, 110602 (2018).
- [43] P. A. Nosov, I. M. Khaymovich, and V. E. Kravtsov, “Correlation-induced localization,” *Physical Review B*

- [99, 104203 \(2019\)](#).
- [44] P. A. Nosov and I. M. Khaymovich, “Robustness of delocalization to the inclusion of soft constraints in long-range random models,” *Phys. Rev. B* **99**, 224208 (2019).
- [45] Xiaolong Deng, Alexander L. Burin, and Ivan M. Khaymovich, “Anisotropy-mediated reentrant localization,” *SciPost Phys.* **13**, 116 (2022).
- [46] A. G. Kutlin and I. M. Khaymovich, “Renormalization to localization without a small parameter,” *SciPost Phys.* **8**, 49 (2020).
- [47] Vedant R. Motamarri, Alexander S. Gorsky, and Ivan M. Khaymovich, “Localization and fractality in disordered Russian Doll model,” *SciPost Phys.* **13**, 117 (2022).
- [48] Weichen Tang and Ivan M. Khaymovich, “Non-ergodic delocalized phase with Poisson level statistics,” *Quantum* **6**, 733 (2022).

Calculation of the probabilities of resonances

Using the parametrization (13) and the left condition in (14), for the box-distributed $\text{Re } \varepsilon_{\mathbf{n}}$ and $\text{Im } \varepsilon_{\mathbf{n}}$ in the interval $|\text{Re } \varepsilon_{\mathbf{n}}|, |\text{Im } \varepsilon_{\mathbf{n}}| < W$, Eq. (2b), we have

$$|X| < 1 - |x|, \quad |Y| < 1 - |y| \quad (21)$$

and the j -resolved probability of usual resonances

$$\begin{aligned}
 P_{res}(j) &= \iiint_{-W}^W \theta(|j| - |\varepsilon_{\mathbf{m}} - \varepsilon_{\mathbf{n}}|) \frac{d\text{Re } \varepsilon_{\mathbf{n}}}{2W} \frac{d\text{Im } \varepsilon_{\mathbf{n}}}{2W} \frac{d\text{Re } \varepsilon_{\mathbf{m}}}{2W} \frac{d\text{Im } \varepsilon_{\mathbf{m}}}{2W} = \iint_{-1}^1 (1 - |x|)(1 - |y|) \theta(J^2 - x^2 - y^2) dx dy = \\
 &= \begin{cases} \int_0^1 (1-x) [2\sqrt{J^2 - x^2} - (J^2 - x^2)] dx, & J < 1 \\ \int_{\sqrt{J^2-1}}^1 (1-x) [2\sqrt{J^2 - x^2} - (J^2 - x^2)] dx + \int_0^{\sqrt{J^2-1}} (1-x) dx, & 1 < J < \sqrt{2} \\ 1, & J > \sqrt{2} \end{cases} = \\
 &= \begin{cases} \pi J^2 - \frac{8J^3}{3} + \frac{J^4}{2}, & J < 1 \\ \frac{1}{3} + \frac{4}{3}(1 + 2J^2)\sqrt{J^2 - 1} + J^2 [\pi - 2 - 4 \arccos(\frac{1}{J})] - \frac{J^4}{2}, & 1 < J < \sqrt{2} \\ 1, & J > \sqrt{2} \end{cases} \quad (22)
 \end{aligned}$$

with $J = |j|/(2W)$.

The plot of the above formula is given in Fig. 2 (blue line) of the main text. One can see that the probability of usual resonances monotonically increases towards 1 with increasing hopping term $J = |j_{\text{mn}}|/(2W)$ with respect to the disorder amplitude W .

The corresponding probability $P_{res}^0(j)$ for the Hermitian case of $Y \equiv y \equiv 0$ as

$$P_{res}^0(j) = \iint_{-W}^W \theta(|j| - |\varepsilon_{\mathbf{m}} - \varepsilon_{\mathbf{n}}|) \frac{d\varepsilon_{\mathbf{n}}}{2W} \frac{d\varepsilon_{\mathbf{m}}}{2W} = \int_{-1}^1 (1 - |x|) \theta(J^2 - x^2) dx = \begin{cases} 2J - J^2, & J < 1 \\ 1, & J > 1 \end{cases} \quad (23)$$

The probability of “bad” resonances is given by the conditions (10), (12), and (14) and takes the form

$$\begin{aligned}
P_{bad}(j) &= \iiint_{-W}^W \theta(|j| - |\varepsilon_{\mathbf{m}} - \varepsilon_{\mathbf{n}}|) \theta\left(1 - \left|1 + \frac{|j|^2}{(\varepsilon_{\mathbf{m}} - \varepsilon_{\mathbf{n}})^2}\right|\right) \frac{d\text{Re } \varepsilon_{\mathbf{n}}}{2W} \frac{d\text{Im } \varepsilon_{\mathbf{n}}}{2W} \frac{d\text{Re } \varepsilon_{\mathbf{m}}}{2W} \frac{d\text{Im } \varepsilon_{\mathbf{m}}}{2W} = \\
&= \int_{-1}^1 \int_{-1}^1 (1 - |x|)(1 - |y|) \theta(J^2 - x^2 - y^2) \theta\left(y^2 - x^2 - \frac{J^2}{2}\right) dx dy = \\
&= \begin{cases} \int_0^1 (1-x) \left[2\sqrt{J^2 - x^2} - (J^2 - x^2) - 2\sqrt{\frac{J^2}{2} + x^2} + \frac{J^2}{2} + x^2 \right] dx, & J < 1 \\ \frac{1}{\sqrt{J^2-1}} \int_0^1 (1-x) \left[2\sqrt{J^2-x^2} - (J^2-x^2) - 2\sqrt{\frac{J^2}{2}+x^2} + \frac{J^2}{2} + x^2 \right] dx + \\ \quad + \int_0^{\sqrt{J^2-1}} (1-x) \left(1 - 2\sqrt{\frac{J^2}{2}+x^2} + \frac{J^2}{2} + x^2 \right) dx, & 1 < J < \frac{2}{\sqrt{3}} \\ \int_0^{\sqrt{1-\frac{J^2}{2}}} (1-x) \left(1 - 2\sqrt{\frac{J^2}{2}+x^2} + \frac{J^2}{2} + x^2 \right) dx, & \frac{2}{\sqrt{3}} < J < \sqrt{2} \\ 0, & J > \sqrt{2} \end{cases} = \\
&= \begin{cases} \left(\frac{\pi}{3} - \frac{1}{2} \ln(2 + \sqrt{3}) \right) J^2 + \left(\sqrt{3} - \frac{5+\sqrt{2}}{3} \right) J^3 + \frac{J^4}{16}, & J < 1 \\ \frac{1}{6} + \frac{2}{3}(1 + 2J^2)\sqrt{J^2 - 1} + J^2 \left[\frac{\pi}{3} - 1 - \ln\left(\frac{1+\sqrt{3}}{\sqrt{2}}\right) - 2 \arccos\left(\frac{1}{J}\right) \right] + \left(\sqrt{3} - \frac{1+\sqrt{2}}{3} \right) J^3 - \frac{7J^4}{16}, & 1 < J < \frac{2}{\sqrt{3}} \\ -\frac{1}{6} + \frac{1+J^2}{3}\sqrt{4 - 2J^2} + \frac{J^2}{2} - \frac{\sqrt{2}}{3}J^3 + \frac{J^4}{8} - J^2 \ln\left(\frac{\sqrt{2}+\sqrt{2-J^2}}{J}\right), & \frac{2}{\sqrt{3}} < J < \sqrt{2} \\ 0, & J > \sqrt{2} \end{cases}. \tag{24}
\end{aligned}$$

The above expression is plotted in Fig. 2 (orange line) in the main text. Unlike the case of the usual resonances, the probability of “bad” ones is non-monotonic and has the maximum at $J \simeq 0.7554$.

These J -resolved probabilities can be used for the calculation of the number of resonances by using the expressions and the parametrization $J_{\mathbf{m},\mathbf{m}+\mathbf{R}} = |s_{\mathbf{m},\mathbf{m}+\mathbf{R}}|/(2WR^\alpha)$, Eq. (15).

$$N_{res} = \sum_{\mathbf{R}} \int P_{res} \left(J_{\mathbf{m},\mathbf{m}+\mathbf{R}} = \frac{s}{2WR^\alpha} \right) P(s) ds \tag{25a}$$

$$N_{bad} = \sum_{\mathbf{R}} \int P_{bad} \left(J_{\mathbf{m},\mathbf{m}+\mathbf{R}} = \frac{s}{2WR^\alpha} \right) P(s) ds, \tag{25b}$$

where the summation over \mathbf{R} is given over the \mathbb{Z}^d -lattice and the averaging over s is taken over the random amplitudes of $s = |j_{\mathbf{m},\mathbf{m}+\mathbf{R}}|R^\alpha$.

From the comparison of the expressions (22) and (23) one can immediately see that the summation over R will diverge at large R (small J) due to the first terms in the above expressions. It is this difference in powers of small- J expansion $P_{res}^0 \sim J$ and $P_{res} \sim J^2$ which shifts the divergence from $\alpha = d$ in the Hermitian case to $\alpha \rightarrow d/2$ (in the absence of “bad” resonances) in the non-Hermitian case.

Both numbers of usual and “bad” resonances in the range $J > 1$ (i.e. at $W > 1/2$ for all $R \geq 1$ and $s < 1$) (25) take the following form

$$N_{res} = \frac{\pi\zeta_{2\alpha}}{W^2} \langle s^2 \rangle - \frac{8\zeta_{3\alpha}}{3W^4} \langle s^3 \rangle + \frac{\zeta_{4\alpha}}{2W^4} \langle s^4 \rangle \tag{26a}$$

$$N_{bad} = \left(\frac{\pi}{3} - \frac{1}{2} \ln(2 + \sqrt{3}) \right) \frac{\zeta_{2\alpha}}{W^2} \langle s^2 \rangle + \left(\sqrt{3} - \frac{5 + \sqrt{2}}{3} \right) \frac{\zeta_{3\alpha}}{W^3} \langle s^3 \rangle + \frac{\zeta_{4\alpha}}{16W^4} \langle s^4 \rangle, \tag{26b}$$

where ζ_x is a zeta function, which converges at $x > 1$.

In order to find the moments $\langle s^q \rangle$, $2 \leq q \leq 4$, one should calculate its distribution. For the box distribution of $|\text{Re } j|$ and $|\text{Im } j|$, Eq. (2b), with the real s_R and imaginary s_I parts of $s = s_R + is_I$ in the interval $|s_R|, |s_I| < 1/\sqrt{2}$, one can find the one of s as

$$P(s) = \iint_{-1}^1 \frac{ds_R ds_I}{4} \delta(s - \sqrt{s_R^2 + s_I^2}) = s \left[\pi - 4 \arccos\left(\frac{1}{\sqrt{2}s}\right) \theta\left(s - \frac{1}{\sqrt{2}}\right) \right] \theta(1 - s). \tag{27}$$

The corresponding moments are given by

$$\langle s^2 \rangle = \frac{1}{3}, \quad \langle s^3 \rangle = \frac{7}{40} + \frac{\ln 2 + 6 \ln(1 + \sqrt{2})}{80\sqrt{2}} \simeq 0.23, \quad \langle s^4 \rangle = \frac{7}{45} \quad (28)$$

After the substitution of $\langle s^q \rangle$ to the above expressions (26), one obtains

$$N_{res} = \frac{\pi \zeta_{2\alpha}}{3W^2} - \frac{\zeta_{3\alpha} [14\sqrt{2} + \ln 2 + 6 \ln(1 + \sqrt{2})]}{30\sqrt{2}W^4} + \frac{7\zeta_{4\alpha}}{90W^4} \quad (29a)$$

$$N_{bad} = \left(\frac{\pi}{3} - \frac{1}{2} \ln(2 + \sqrt{3}) \right) \frac{\zeta_{2\alpha}}{3W^2} + \left(\sqrt{3} - \frac{5 + \sqrt{2}}{3} \right) \left[\frac{[14\sqrt{2} + \ln 2 + 6 \ln(1 + \sqrt{2})]}{80\sqrt{2}} \right] \frac{\zeta_{3\alpha}}{W^3} + \frac{7\zeta_{4\alpha}}{720W^4}, \quad (29b)$$

coincide with the approximate expressions (16) and (17) in the main text. The expressions for $W < 1/2$ are straightforward to calculate from (25), (22), and (24), but have quite cumbersome analytical expressions.

Like in the Hermitian case at $\alpha < d$, where the presence of the extensive number of resonances N_{res} per eigenstate breaks down the spatial renormalization group [10], in the non-Hermitian case the presence of a small fraction of “bad” resonances per eigenstate does this job.

Indeed, the spatial renormalization group [10] is based on the assumption that one can hybridize the resonance pairs one by one, going from the strongest ones (at smaller distances) to the weaker ones (at larger distances) and never coming back to the same (previously resonant) pair, due to its hybridization.

In the non-Hermitian “bad” resonances, the situation is drastically different as each of such resonances attracts the levels even closer via hybridization. This opens the possibility of the recurring resonance pairs at later stages of the renormalization group and, thus, to the avalanche of resonances. To avoid having such avalanche effects, one needs to have the number of resonances per eigenstate small enough. We estimate this number numerically in the main text.

Numerical results

In this section, we show further numerical data to support our claims. In particular, in the main text, we consider the inverse participation (IPR) ratio for the right eigenvector. Now, we consider the more generally defined as

$$IPR_2 = \sum_{\mathbf{m}} |\psi_n^r(\mathbf{m})|^2 |\psi_n^l(\mathbf{m})|^2, \quad (30)$$

where ψ_n^r and ψ_n^l are the right- and left- eigenvectors. D_2 is the respective fractal exponent

$$D_2 = -\frac{d \log IPR_2}{d \log N}. \quad (31)$$

Figures 7(a)-(b) show IPR_2 and D_2 . These panels should be compared to Figs. 4(c)-(d), where we computed for the same value of W and b the right IPR_2^r and D_2^r . We do not observe any substantial changes and $D_2^r \approx D_2$. Furthermore, in Fig. 7, we show IPR_2 and D_2^r for the Hermitian case. For the Hermitian case, we keep the diagonal disorder strength having the same magnitude as the absolute magnitude of the non-Hermitian one. The Hermitian case is more delocalized compared to its non-Hermitian counterpart. At the Anderson critical point $\alpha_{AT} = 1$ the fractal dimension shows multifractality ($0 < D_2^r < 1$) for the Hermitian case, while for the non-Hermitian one $D_2^r \approx 0$, see dashed black for reference.

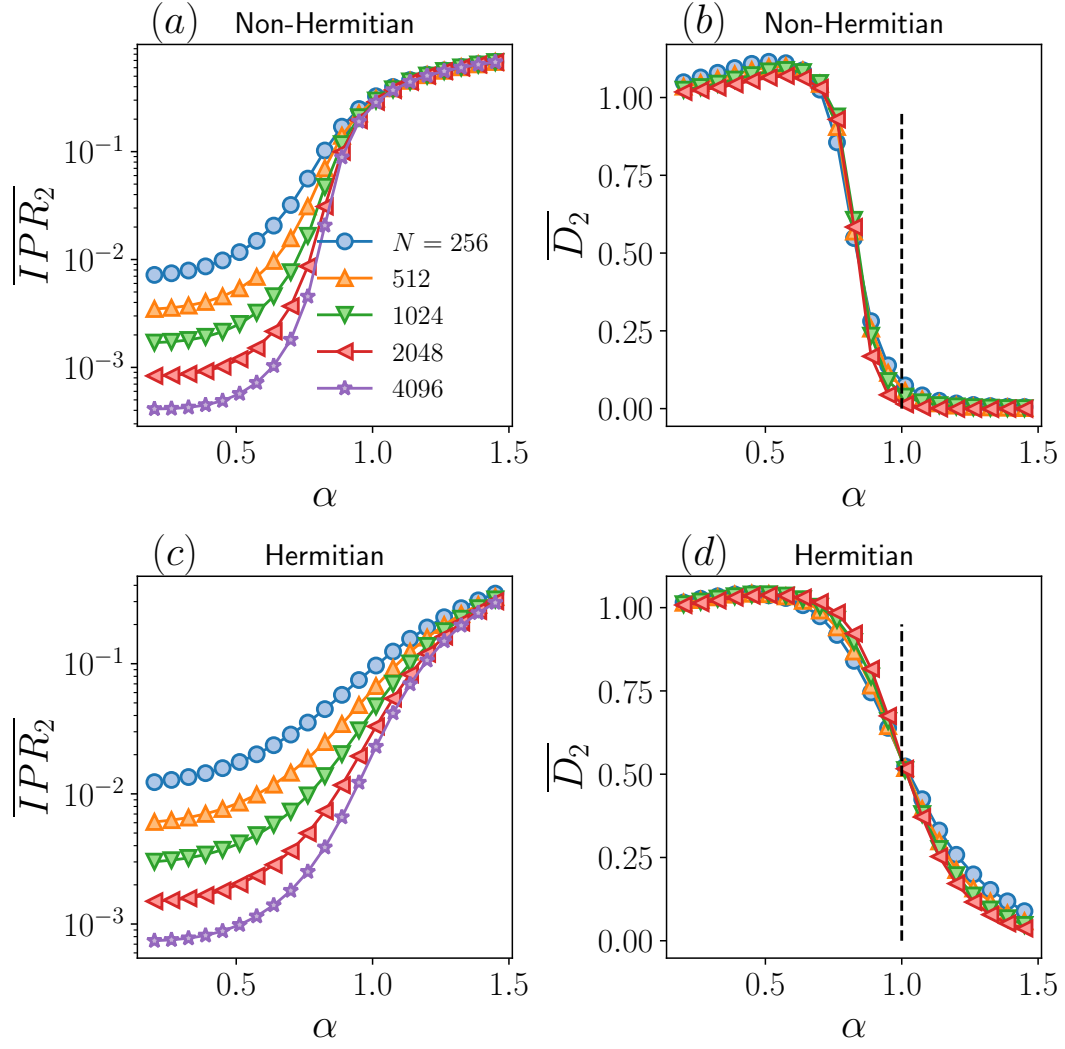


FIG. 7. (a),(b) \overline{IPR}_2 and \overline{D}_2 vs α for $W = 2$ and several N for the non-Hermitian model. (c),(d) \overline{IPR}_2 and the respective fractal dimension \overline{D}_2 for $W = 4$ for the Hermitian case. The vertical dashed line $\alpha_{AT} = 1$ points the phase transition in the Hermitian case.